Measurement of optical refraction-, transmission- and turbulence effects in the False Bay, South Africa; June 2007

Arie N. de Jong, Piet B.W. Schwering, Peter J. Fritz,
TNO-Defence, Security and Safety, The Hague, The Netherlands

ABSTRACT

Complementary to a measurement campaign of small surface targets in the False Bay, South Africa [1], a set-up could be arranged of atmospheric propagation experiments. This opportunity allowed us to collect another set of transmission data in a coastal area, where the environmental conditions are generally non-homogeneous and rapidly changing. It was found before, that the validity of models, predicting the aerosol size distribution, the vertical temperature profile or the structure constant for the refractive index C_n^2 tends to be questionable in this type of areas [2,3]. Proper knowledge of the relation between the range performance of electro-optical and infrared sensors and in-situ weather parameters is however of key importance for operational use of this type of sensors, so the collection of additional propagation data was very relevant. Refraction data were collected continuously by using a geodetic theodolite with camera system over a 15.7 km path in the False Bay. Transmission- and scintillation data were collected over a 9.6 km path by means of our MSRT (Multi-Spectral Radiometer Transmissometer) and a Celestron telescope (with camera) with a focal length of 1.25 m. Weather parameters were measured at a shore station and on a rock in the bay. The weather was greatly variable with many showers, while the visibility, cloudiness and ASTD (Air-Sea Temperature Difference) conditions were continuously changing. Analysis of the theodolite data delivered absolute AOA (Angle of Arrival) data, which have been compared with predictions from the bulk model for marine boundary layers and from two empirical two-parameter temperature profiles. Transmission data, collected in three spectral bands (around 0.6, 0.9 and 1.5 μm), provided information on the particle size distribution, assumed to be of a Junge type. Knowledge of this information allows the prediction of the atmospheric transmission in other spectral bands, including the IR. The transmission data were compared with the data from a visibility meter on the roof of the IMT building. Both data sets correlated reasonably well. From the high speed MSRT transmission data (integration time 10 ms, sampling rate 30 Hz) the scintillation index (SI) was calculated, which showed a reduction in SI value when it starts to rain, while the SI came back to normal shortly after the shower. The measured SI data were transformed into C_n^2 values (the atmospheric refractive index structure function) and compared with predictions from the bulk model with different type of stability functions for a selected set of measurement periods. The model predictions show deficiences for conditions with small ASTD. The SI data from the MSRT were compared with the scintillation data, collected with the Celestron imaging system, which showed interesting correspondences and differences, which are discussed in the paper. From the Celestron data also the beam wander was determined, providing, similar to the SI, a source of information on C_n^2. It was shown, that the beam wander (blur) also correlates with ASTD.

Keywords: atmospheric transmission, refraction, aerosols, particle size distribution, scintillation, beam wander, blur

1. INTRODUCTION

Since recent developments of optical and infrared sensor systems, the spatial resolution and sensitivity has continuously been improved up to limits, where the atmosphere becomes the dominant factor. Refraction and turbulence effects cause distortion and blurring, reducing the capability of target identification for imaging sensors and the performance of laser systems, such as used in laser communication, target designation and directed energy weapons. Furthermore atmospheric aerosols cause increased loss in target contrast for longer ranges. On the other hand refraction and scintillation may lead to higher signal levels and thus enhanced target detection capability. These days, coastal areas are becoming of greater importance, for example due to the increase of the number of invading people. As a consequence we spent considerable effort in the measurement of atmospheric propagation effects. Experiments have been carried out in the Baltic Sea [4], in the Mediterranean [5], the San Diego Bay [6], the Persian Gulf [7], Hawaii [8] and in the Chesapeake Bay [2], where in each experiment the data base was enhanced and the accuracy of predicting models such as EOSTAR [9] improved.

Optics in Atmospheric Propagation and Adaptive Systems XI, edited by
Anton Kohnle, Karin Stein, John D. Gonglewski, Proc. of SPIE Vol. 7108
710803 · © 2008 SPIE · CCC code: 0277-786X/08/$18 · doi: 10.1117/12.797460

One remarkable effect of atmospheric refraction is intensity gain due to focussing. The magnitude of this effect can be investigated by assuming a vertical temperature profile and performing precision ray tracings. Variations in the profile due to the passage of a cold front, such as occurring during the Baltic '99 trial, are good illustrations of this method [10]. Similarly such a passage leads to changes in the geometrical distortion, as illustrated during the POLLEX trial [5,11]. In these cases we used a buoy with one or more temperature sensors, somewhere midpath located, for collecting data on the ASTD. Problems were faced with obtaining a reliable air temperature at low height (<1m), the surface temperature of the water and with enough relative accuracy (<0.01 K). In the SAPPHIRE trial [2]we could get the required accuracy for an array of temperature sensors on the buoy, so for the first time we could measure the temperature gradient, which made possible the application of a set of empirical profiles. Measured and predicted distortion could be compared, where it was found that in the Chesapeake Bay a power type profile fitted much better than profiles generated by the bulk method. It is noted, that enhanced detection ranges for point targets at the horizon can be obtained by the refraction effect [12].

The challenge on aerosols was to find out their nature in coastal areas, potentially influenced by breaking waves in the surf zone and the direction of the wind: off-shore or on-shore. It was found, that the paricle size distribution fits nicely to the Junge type. By measurement of multi-band transmission data, the parameters of the Junge distribution (exponent and coefficient) can be obtained with reasonable accuracy [3, 4]. Another issue of importance is the inhomogeneity along the path. One way to investigate this is the use of locally operating visibility meters and compare their data with those of the transmissometer. During the VAMPIRA trials [13] a poor correlation was found, indicating strong inhomogeneity across the Bay. Scintillation due to atmospheric turbulence has been studied intensively because of the program on point target detection. It is noted that other effects may introduce strongly fluctuating signals in detection sensors, for example waves at the surface [14], sometimes hard to be separated from turbulence effects. In the LAPTEX [15], EOPACE [16,17] and POLLEX [5] trials scintillation levels were obtained for operationally interesting ranges (15-25 km). Data were collected with modulated sources detected by a transmissometer, as well as DC sources, observed with a camera (IR or visual). In various cases differences were found, probably due to pupil averaging. Another turbulence effect concerns atmospheric blur, including beam wander, for which it is difficult to find correlations with weather data. This effect directly relates to the spatial resolution of camera's. The trials in the False Bay (Western Cape of South Africa, see Figure 1) in June 2007 (local winter time) provided an excellent occasion for further quantification of several of the beforementioned effects.

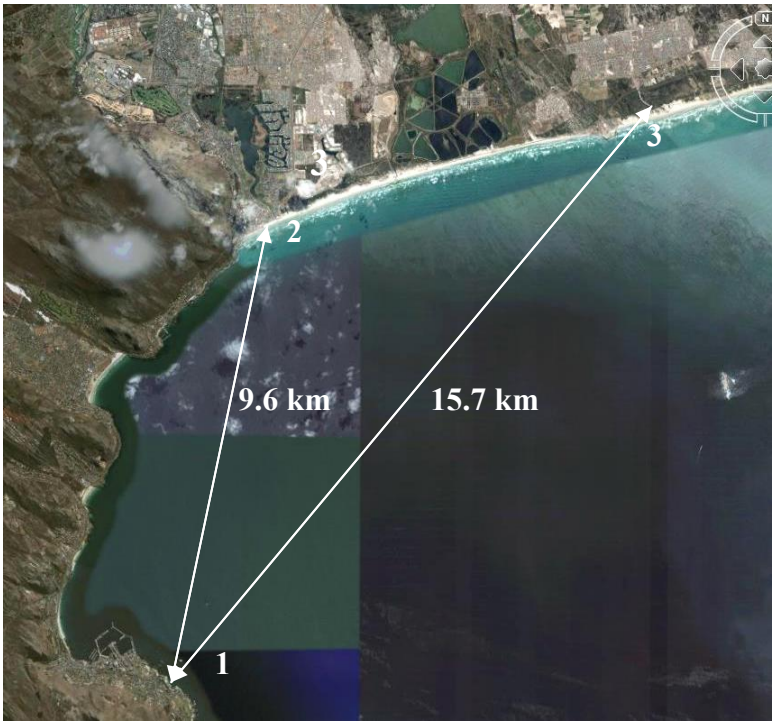

Figure 1. Situation sketch of the measurement paths in False Bay (South Africa): 1 = IMT near Simonstown; 2 = Empire buiding at Muizenberg; 3 = Rescue building near Strandfontein (picture from Google Earth)

2. INSTRUMENTATION

The False Bay, located at the border of the warm Indian Ocean and the cool Atlantic Ocean, provides ideal opportunities for trials on signatures of maritime and coastal targets and atmospheric propagation. In Figure 1, three locations are shown for our propagation experiments: IMT, where we installed the Celestron, the theodolite and the source of the MSRT, the Empire building for the MSRT receiver and the Celestron source and the rescue building for the theodolite source. Images of these devices are shown in Figure 2. A weather station from IMT was installed at Roman Rock, a small island at 1.8 km distance from IMT and a weather station from TNO (including rain and cloud recording) was installed on the roof of IMT. The water temperature was measured at several buoys and at Roman Rock. An IMT (Vaisala FS2) visibility meter was located at the roof of IMT. The geodetical coordinates for IMT are: 34°11'33.06"S, 18°26'43.80"E.

Figure 2. Instruments, located at IMT (left): the Celestron, MSRT source and theodolite; at the Empire building (centre): the MSRT receiver with rain protection; at rescue building (right): one of the two sources for the theodolite

The Celestron telescope, located at 8.5 m above sea level, has a focal length of 1250 mm and a pupil size of 125 mm. The standard 1/2" CCD camera has a chip size of 6.4x4.8 mm, providing a Field of View (FOV) of 5.12x3.84 mrad and a pixel size of about 6.7 µrad. The images were recorded in series of 50 consecutive full frames (100 half frames) each 10 minutes by means of a standard frame grabber. During local analysis, for each of the splitted frames the sum of the pixel values compared to the background level was calculated (including the average and the variance for the 50 sums), as well as the centre of gravity. The Celestron was aimed at a DC halogen lamp (diameter 8.6 cm) at Empire (distance 9.6 km, 7.5 m above sea). The exposure time for the camera was set to 0.1 ms, providing a very low background radiance level, while with a gain setting of 48 the source signal level did never saturate.

Behind the eye-piece of the Topcon AT-G2 theodolite (magnification of 32x) a Sony CCD camera type XC/73CE (chip size: 4.89x3.64 mm) was mounted together with a 22.5 mm objective lens. Because of dynamic range, the shutter time and the gain were set to an appropriate level. In the image a cross-hair is aiming at the geometrical horizon. The height, at which the sources at 15.7 km are observed with respect to the cross-hair, indicates the refraction properties in the intervening atmosphere. The vertical FOV in the CCD image is about 5.0 mrad, about ¼ of the optical FOV of the theodolite. Each minute 5 consecutive frames were grabbed. After one day a total of 7200 frames was stored on a dvd. The sources were provided with two 50 W DC lamps in the focus of 15 cm reflectors, mounted at 8.7 m above sea level. The theodolite was at 7.9 m above sea level. The MSRT transmissometer (for details see: [3],[4],[6],[7] and [13]) was installed at the balcony (first floor, room E113), at 8.0 m above sea. The source height was 8.1 m. Only three of the spectral bands of the MSRT were used: 0.57-0.65 µm, 0.78-1.04 µm and 1.39-1.67 µm, providing estimated, appropriate S/N ratios for the 9.66 km range: resp. 150, 900 and 600 for an integration time of 10 ms. The reference signal of the source (1000 Hz) was transmitted by radio link to the receiver location.

3. REFRACTION MEASUREMENTS AND MODELING

Most of the time in the measurement period (3-16 June), refraction data could be collected. Some data were lost due to poor visibility or contrast, power failure or mis-alignment. Figure 3 shows the results of the measured difference in Angle of Arrival (Delta AOA) between the absolute AOA with the geometrical horizon and the neutral AOA, defined here as the AOA in conditions of standard pressure- and adiabatic temperature decrease (6 K/km) with height. For the path of 15.7 km and the given source- and receiver heights the neutral AOA has a value of 0.971 mr. The figure also shows the ASTD for the period, measured at Roman Rock. Some uncertainty exists about the water temperature, because in many cases the surface (skin) temperature may deviate from the bulk temperature, depending on the mixing effects in the upper water layers. Another uncertainty concerns the constancy of the ASTD over the path-length. For the air temperature we found very good agreement between the data from Roman Rock and the IMT roof (difference generally smaller than 0.1 K). For the water temperature greater differences were found. In any case, it was shown before [2], that the air-temperature gradient at about the heights of the source and the receiver is the dominant parameter.

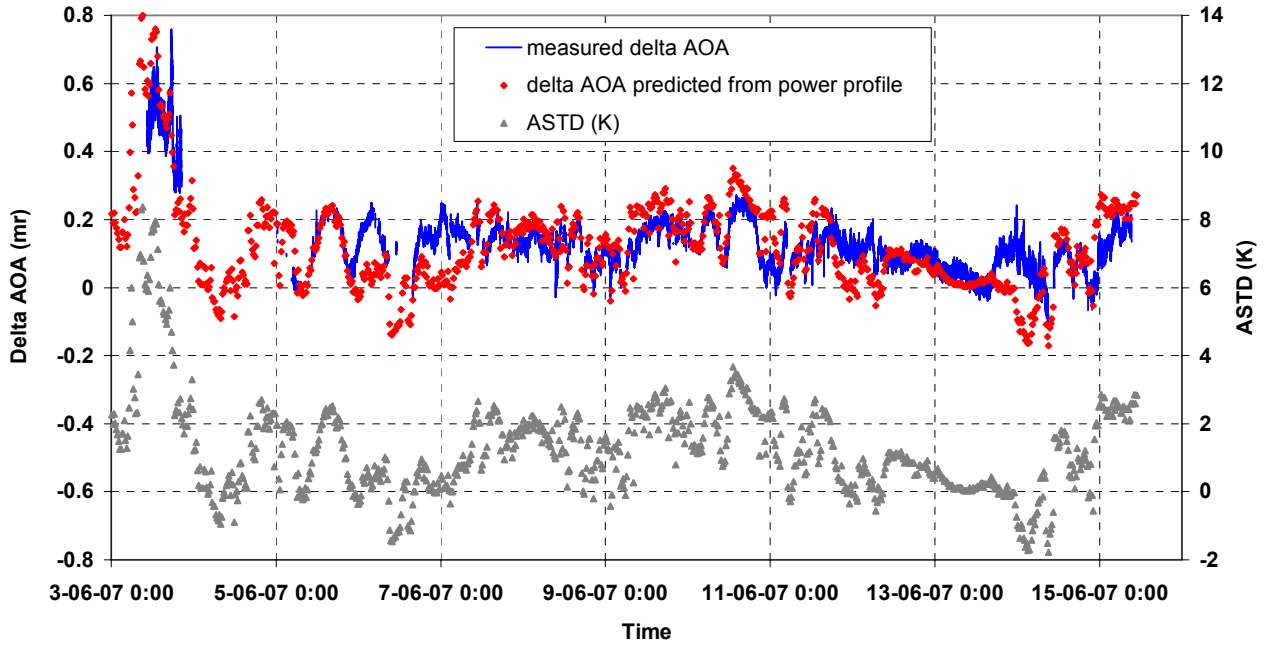

Figure 3. Plots of measured and predicted AOA difference with neutral direction and ASTD for the whole trials period

An attempt was made to predict Delta AOA from the ASTD by using an empirical two-parameter profile similar to the method used in [2]. If T is defined as the temperature difference at heights h and 0 (basically ASTD), we used the profile given by $T=a*h^n$, with the associated gradient T', given by $T'=n*a*h^{n-1}$, and the ratio $T'/T=n/h$. Several values for n and h in this so-called power profile were tried, where it was found, that for a ratio $T'/T=0.15$ at a height of 10 m, the following relation exists between T (ASTD) and Delta AOA: Delta AOA=0.0955*T+0.0059 (mr). This empirical relationship is resulting from precision ray-tracings, as described in [10]. The result of this prediction is also shown in Figure 3. The agreement between measured and predicted data is generally rather good, including for the positive ASTD conditions of the 3rd of June. It appeared, that the exponential profile $T=c*\{1-\exp(-a*h)\}$ with the two selectable parameters c and a, does not work correctly for positive ASTD conditions. Furhermore this profile predicts mirages for ASTD's smaller than -1K, while the source is below the apparent horizon. During the trial no mirages were observed from the source at the rescue building. Also the temperature profiles, predicted by the bulk model for the Marine Boundary Layer (MBL) as implemented in the EOSTAR program were investigated, using the EOSTAR ray-tracing scheme. Running this program with the bulk model according to Smith and two models for the stability functions (Paulson and Kondo), we found the following two approximating relationships between Delta AOA and T: Delta AOA=0.043*T-0.0906 (Smith/Kondo) and Delta AOA=0.162.4*T-0.0869 (Smith/Paulson). We concluded, that for the whole trials period, the Smith/Paulson model gives a better agreement with the measured data than the Smith/Kondo model.

This result is different from the results in the Chesapeake Bay [2], where the profile from the Smith/Paulson model did not give a good agreement with the measured AOA's, especially for the positive ASTD conditions. This was also the case in False Bay. The correspondence of the prediction for Smith/Kondo is poor: the predicted Delta AOA's are far too small. It might be that a modification to the Kondo stability functions, as presented by Claverie [18] for the VAMPIRA data, would give better results. It appears from Figure 3, that the prediction is inaccurate during some short periods, far outside the error bar area of the measured Delta AOA (~0.013 mr). Examples are the periods: 5 June 22.00-6 June 07.00; 6 June 19.00-7 June 08.00 and 13 June 18.00-14 June 07.00. Analysis of the weather data shows, that in these periods, the windspeed decreases to values below a few m/s. Apparently the temperature profile becomes distorted in these cases, so that the gradient at appropriate heights is less than predicted by the models and the measured AOA is higher than predicted. In the example of 13 June, for the period after midnight, the wind direction changed in combination with the low windspeed, from South-East to South-West, resulting apparently in a negative measured ASTD (incorporating a predicted negative Delta AOA), while we measured a positive Delta AOA. We can conclude, that in the procedures of predicting temperature profiles, we must be careful in conditions of low windspeed and variable wind directions.

4. TRANSMISSION MEASUREMENTS AND MODELING

The raw data from the MSRT transmissometer were stored in 10 minute files with 18000 samples of data for each of the channels. In the data processing offset voltages of 6.5, 4.9 and 5.9 mV were subtracted from the measured signals. The next action was the conversion of the data into total transmission values. In this procedure raw calibration was carried out with conversion factors from previous trials. It was found from the comparison of the transmission behavior in the three channels, that in periods of good visibility the type of aerosols was rural and not of the Navy Aerosol Model (NAM) type with any of the Air Mass Parameters between 1 and 10. We had to split the data into two sets, before and after the 10th of June, the day that the lamp in the source was exchanged. As calibration times we took: 5 June 17.10 and 13 June 06.00. The air temperatures were respectively: 15.4 and 13.4 C; the relative humidities: 53 and 54 % and the visibilities: 40 and 100 km. With these parameters MODTRAN was run for a range of 9.66 km, resulting in transmission values of 0.437, 0.495 and 0.447 respectively 0.717, 0.672 and 0.521 for both calibration times and for the three channels around 0.6, 0.9 and 1.5 µm. The calibration voltages for both cases were 2.19, 0.70 and 0.70 V respectively 2.65, 0.778 and 0.822 V. Total transmission values were obtained by dividing the measured voltage by the calibration voltage and multiplying by the calibration transmission.

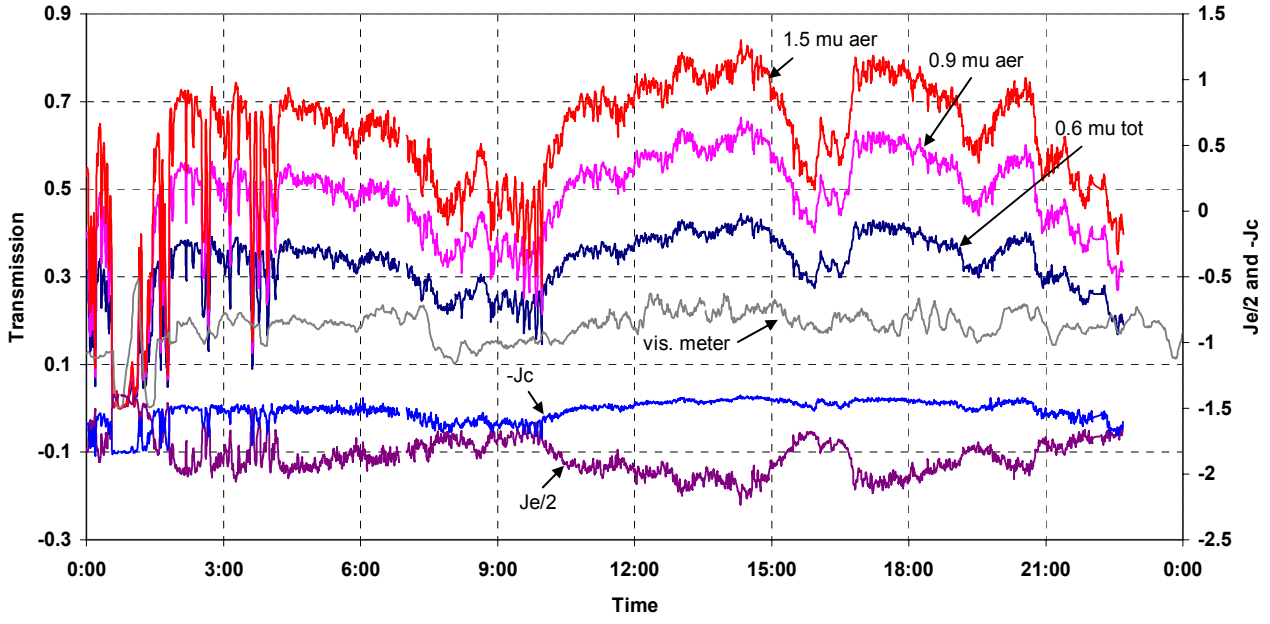

Figure 4. Transmission data for the 5th of June, including plots of retrieved data for J_e and J_c (1 minute-averaging).

Total transmission values were split into the contribution from molecular extinction and from aerosol extinction. For this reason the absolute humidity AH was calculated from the air temperature T and relative humidity RH by means of the approximation: AH=RH*{0.02 *T^2+0.1874*T+5.5304} (g/m^3). For values of AH between 6 and 12 g/m^3 we can use the following approximations for molecular transmission: 0.923-0.0024*AH, 0.838-0.0104*AH and 0.59-0.006*AH for the three spectral bands around 0.6, 0.9 and 1.5 µm. Next the aerosol transmission was calculated by dividing the total transmission by the molecular transmission. Examples of both types of transmission are shown in Figures 4 and 5 for the dates 5 and 11/12 June. The figures also show the transmission τ, obtained from the IMT visibility meter by means of the formula: $\tau = \exp\{-3.91*9660/R\}$ where R is the measured visibility range in m. The transmission by aerosols only was used to characterise the particle size distribution of the aerosols, following the method explained before ([3], [4]) and based upon the simple Junge type distribution. This distribution is based upon the formula: $\log(dN/dD)=J_c+J_e*\log(D)$, in which J_c and J_e are the Junge coefficient respectively Junge exponent and D the particle diameter. In the extraction method the average τ(av) of the transmission values τ_1 and τ_2 in the centres of two neighboring spectral bands are taken and the slope $s(t)=(\tau_1-\tau_2)/(\lambda_1-\lambda_2)$, where λ_1 and λ_2 are the centre wavelengths. The value of J_e is determined from the relation: $J_e=s(J_e\text{-}t)*s(t)-2.78$, where $s(J_e\text{-}t)$, the slope in a set of plots of given J_e values against τ(av), is related to τ(av) by the relation: $s(J_e\text{-}t) = -2.85*\{tg(90*\tau(av))\}^{-0.53} - 2.75*\{tg(90*\tau(av))\}^{0.87} +1.80$. We have taken here the spectral bands around 0.91 and 1.53 µm, because the data are somewhat more consistent in this band combination than in the other band combination. The value of J_c is determined by the relation: $J_c=-1.544*\tau(av)+d$, where $d=-0.209*J_e^2-1.956*J_e-2.005$ for the range of 9.66 km. The retrieved values of J_e and J_c are also plotted in figures 4 and 5.

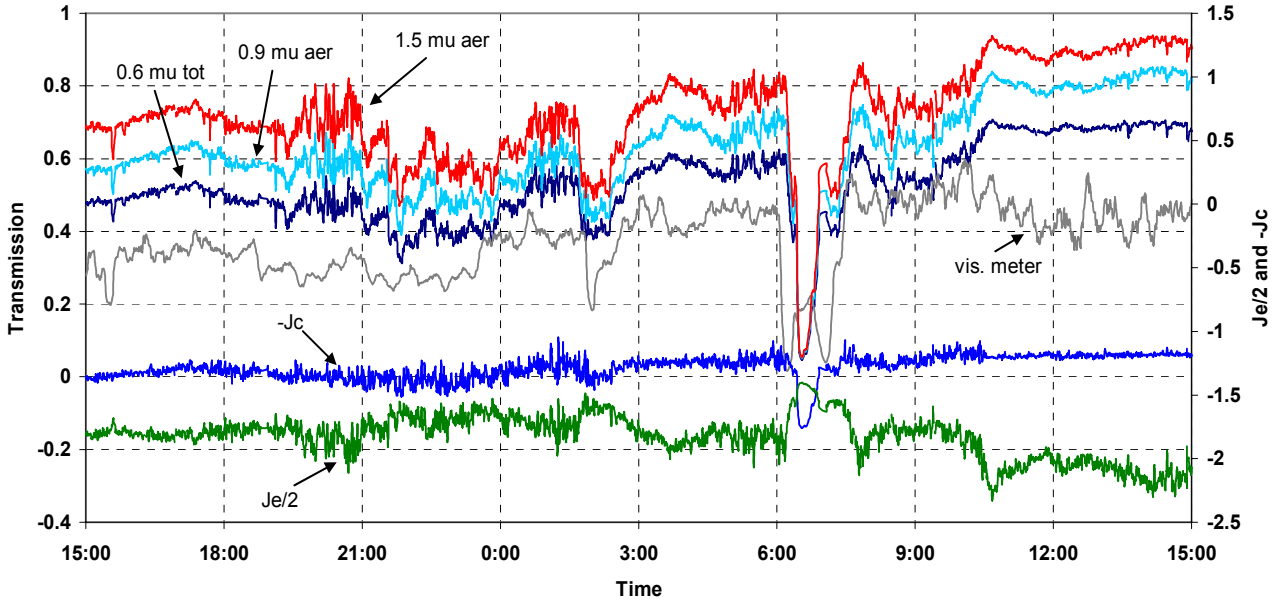

Figure 5. Transmission data for 11 June 15.00 to 12 June 15.00 (1 minute-averaging).

For the transmission plots, shown in figures 4 and 5, we applied a one minute averaging with two samples per minute. The plots show clearly variations in transmission values, mainly due to showers and changes in visibility conditions. In the early morning of the 5th, the showers are of short duration (a few minutes), while in the morning of the 12th, the duration of the shower is about 25 minutes. It is interesting to note the double peak in the plot from the visibility meter. The transmission values, obtained from this instrument are systematically lower than those of the MSRT, probably due to the fact that the visibility meter did locally measure more aerosoles from the coastal zone, while the path from IMT to Empire contained in general a cleaner atmosphere. To obtain a clearer view of the transmission behavior during rain, we have presented a three hour period on the 8th of June, with 11 showers in Figure 6. Rain gauge measurements show that most of the showers are local events of short duration, so the correlation between the extiction coefficient and the rain rate is poor. The fact that the 0.6 and 1.5 µm transmission values remain proportional during rain, indicates that the extinction coefficient is wavelength independent and that the particles in the air are large (> 0.1 mm).

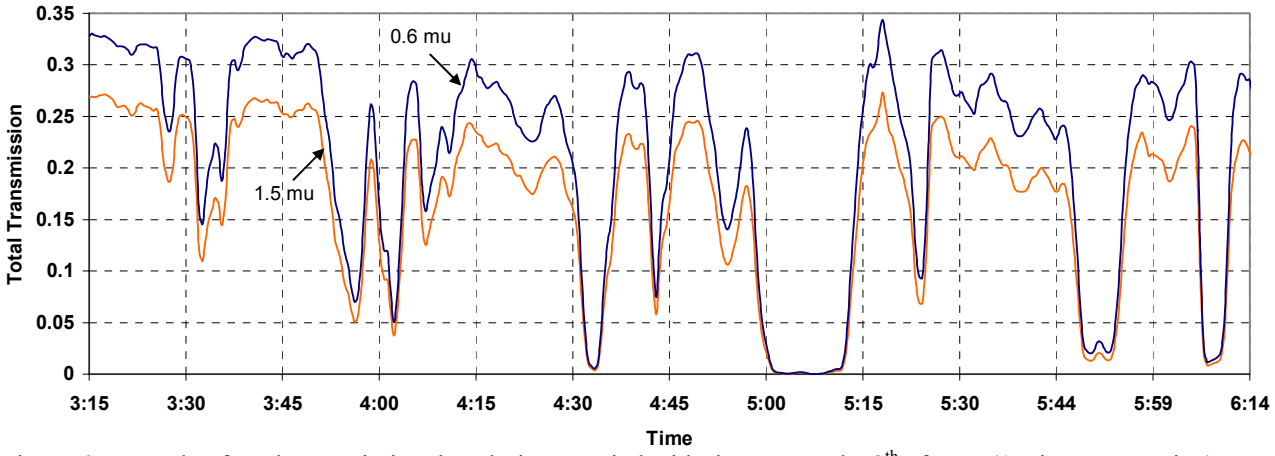

Figure 6. Example of total transmission data during a period with showers on the 8th of June (1 minute-averaging)

Following the MODTRAN rain model, taking the Marhall-Palmer size distribution: $dN/dD=N_0*\exp(-4.1*D*\rho^{-0.21})$, the transmission due to rain only is determined by the relation: $\tau(rain)=\exp(-0.365*R*\rho^{0.63})$, where $N_0=8000$ ($mm^{-1}m^{-3}$), D is the drop diameter (mm), R the range (km) and ρ the rain rate (mm/hr). For a rain rate of 1 mm/hr we find a transmission level over a 9.66 km path of 0.029. Our rain gauge (Tipping Bucket type: HB 3166-02 from Casella) did measure around 04.00 a rain rate of 20 mm/hr and around 05.50 a rain rate of more than 40 mm/hr, while at other signal dips (for example at 05.05) no rain was measured, which indicates again that most of the showers were very local events. This corresponds to the short duration (a few minutes) of the showers, because a shower of 2 km wide drifting by at a cross windspeed of 10 m/s would last about 3 minutes.

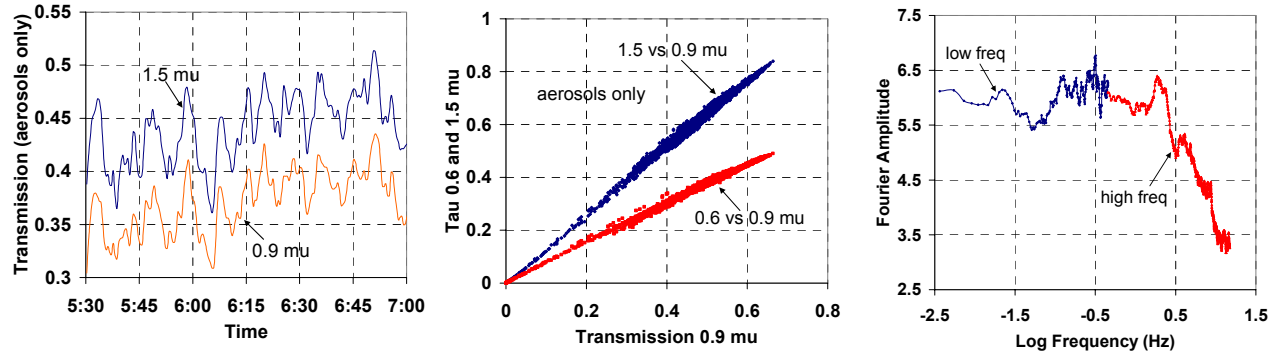

Figure 7. Gravity waves on 7 June (left), plots of transmission in one band versus the other bands for 5 June (centre) and Fourier spectrum for 12 June 05.40 (10 minute period, data taken at high sample rate)

Other results from the analysis of the transmission experiments are shown in Figures 7 and 8. Gravity waves (Fig. 7 left), producing variations in atmospheric conditions were found at several occasions. Correspondence was found with cloud imagery from the MODIS (aqua/terra) camera's from NASA, on which periodical clouds streets were frequently visible. Excellent correlation of the transmission values in the different bands for a full day of data (5 June) is shown in Figure 7 (centre). The correlation plots in this figure are based upon an averaging time of one minute. The temporal spectrum of the data at high sample rate, shown in Figure 7 (right), shows a flat behavior up to a frequency of 2 Hz; above this frequency the ampltude drops a factor 2 per decade or with $f^{-0.5}$, which is a less steep drop-off than the Kolmogoroff spectrum ($f^{-8/3}$). Figure 8 (left) shows the effect of integration time on the correlation coefficient for a selected data-set under moderate turbulence conditions (std/avg=0.36). The remaining correlation coefficient for the smallest integration time of 10 ms is about 0.3. The histogram of 10 minutes of transmission data, shown in Figure 8 (centre), illustrates how well the logarithm of the transmission data fit to a Gaussian type of curve. In Figure 8 (right) we find how much the maximum transmission values exceed the average values, which is of importance to staring-IRST designers.

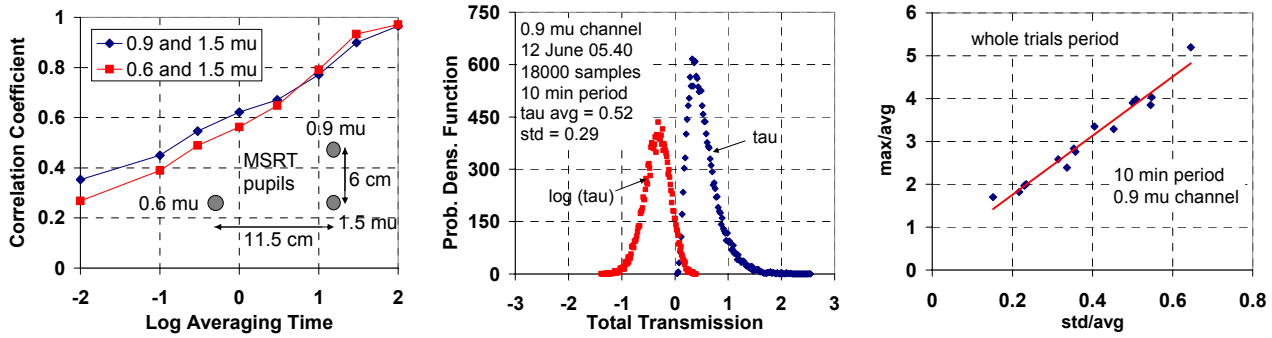

Figure 8. Correlation coefficient versus averaging time for 3 MSRT channels for 5 June 21.00 (10 minute period, left), histogram for a 10 minute data series on 12 June 05.40 (centre) and max/avg versus std/avg for a selection of periods of 10 minutes during the whole trial with different turbulence conditions (right).

5. SCINTILLATION AND BEAM WANDER

Before starting the analysis of the data on scintillation and beam wander we will have a brief look to the qualitative and quantitative predictions of the bulk model, as implemented in EOSTAR [9]. This model gives plots of the C_n^2 ($m^{-2/3}$), the refractive index structure function of the atmosphere, and blur (μrad) as function of altitude (Figure 9, left). The model, showing a decrease of both effects with altitude, has been run for various values of ASTD and windspeed (v). It was found that the Smith's bulk model with Paulson's stability functions, giving reasonable results for the prediction of refraction, did not work well for scintillation, so we took the Kondo variant in this case. In Figure 9 (centre), the variation of C_n^2 (Smith/Kondo) and blur (Smith/Paulson) with ASTD is shown for a wind speed of 5 m/s. C_n^2 is calculated for an altitude of 6.3 m, which is about the minimum height of the line between source and receiver. For the other relevant parameters we took: sensor and source at 8 m altitude, range 9.66 km, relative humidity: 70%, sea temperature: 16 C, atmospheric pressure: 1014 hPa. It appears, that the model predicts a minimum in C_n^2 and blur for an ASTD value around +0.75 K. This phenomenon can nicely be validated with our data, collected at the False Bay trial. It must be stated, that the "dip" effect is non-natural, as we expect the ASTD to vary over the range with maybe more than 1 K, so probably most of the dip is smoothed. In Figure 9 (right), the dependence of C_n^2 and blur (taking Smith/Kondo) with windspeed is shown for two values of ASTD (-2 and 0 K). The model predicts a serious drop in C_n^2 and blur values for windspeeds below 2 m/s, which is corresponding to the feeling, that turbulence is wind driven: more wind means more turbulence. The blur in this model is calculated according to the method, used in Beland [19], in which the blur is defined from the cut-off frequency (1/e point) of the atmospheric MTF and found to be related to the range R, the wavelength λ and C_n^2 by: $c*\{\lambda^{-1/3}*(C_n^2*R)^{0.6}\}$ (μrad), where c is a constant. In our example we took for λ: $0.6*10^{-6}$ m and for R: $9.66*10^3$ m. The blur (long term exposure), shown here, includes beam wander and small scale blur.

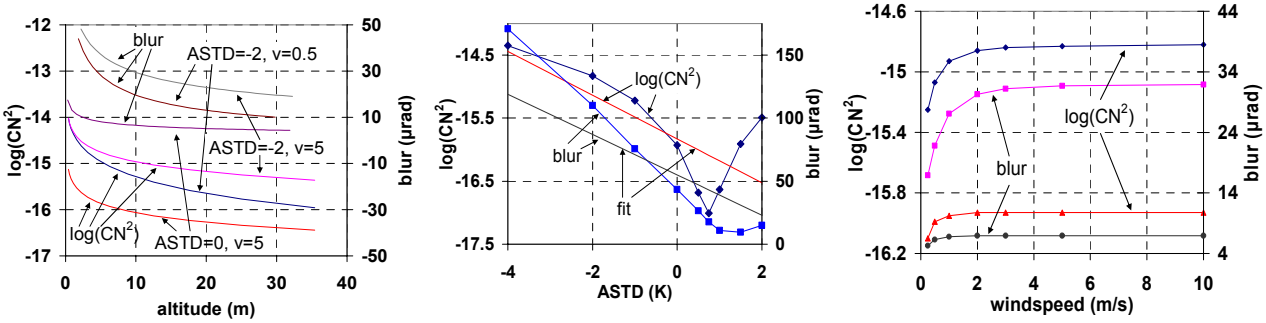

Figure 9. Predictions of log (C_n^2) and blur behavior (as function of environmental parameters) from the bulk model of Smith/Kondo; left: as function of altitude for ASTD's of 0 and -2 K and windspeeds of 0.5 and 5 m/s; centre: as function of ASTD with lines of experimental fit; right: as function of windspeed for ASTD = -2 K (above) and 0 K (below)

For the investigation of the Scintillation Index (SI), defined by the ratio $(std/avg)^2$, raw transmission data were processed in a similar way as in the procedure, described in section 4. The standard deviation was calculated for 300 samples (10 s), averaged over 10 s and sampled 18 times per minute. Then the average over 1 minute was taken, which was sampled two times per minute. Examples of the effect of ASTD and windspeed on SI are shown in Figure 10 for three nine hour periods with "clean" weather without showers. In the plots of the left figure the windspeed is about constant (high), while the ASTD is increasing. We find, that the SI is decreasing, corresponding the trend in Figure 9, but without the "dip" effect. The plots in the centre of Figure 10 show a constant ASTD and decreasing windspeed, resulting in an increasing SI, which is the contrary of the prediction of Figure 9 (right). In the plots on the right of Figure 10, the ASTD and windspeed are both slightly increasing, resulting in SI values between 0.2 and 0.3, except in the period between 02.50 and 04.00, when the windspeed drops to zero and SI therefore increases to values above 0.3.

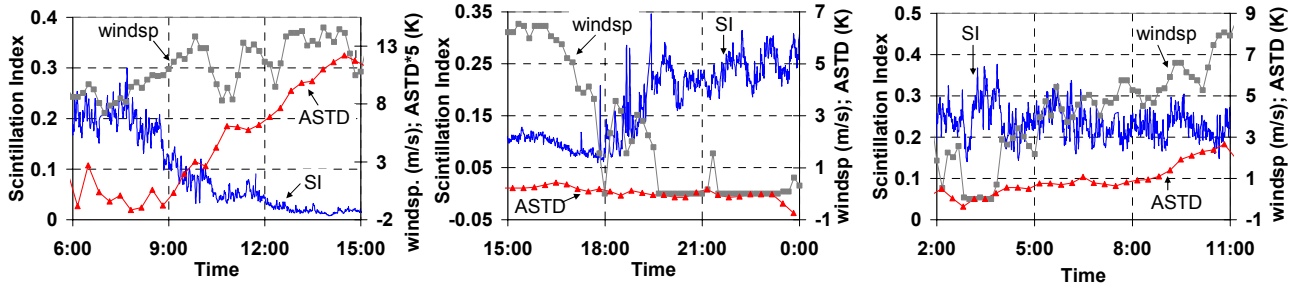

Figure 10. Examples of the influence of ASTD and windspeed on the Scintillation Index (SI) on 5 June (left) with high windspeed and increasing ASTD (decreasing SI), 13 June (centre) with constant ASTD and decreasing windspeed (increasing SI) and 7 June (right) with increasing ASTD and windspeed (about constant SI).

From this type of results we determined an empirical relationship between SI and ASTD via the "fit" line for $\log(C_n^2)$ in Figure 9 (centre): $\log(C_n^2)=-0.347*ASTD-15.83$ and a relation: $SI=12.7*10^{14}*C_n^2$, which is considered for a wavelength of 0.9 μm and a range of 9.66 km. If we compare the latter relation with the prediction for a plane wave (Beland p. 185 [19]): $SI=\sigma_I^2=4*\sigma_\chi^2=1.23*(2\pi/\lambda)^{7/6}*(R)^{11/6}*C_n^2=24.0*10^{14}*C_n^2$, and for a spherical wave: $SI=9.68*10^{14}*C_n^2$, we find that the approximation, we used, is closer to the theoretical prediction of SI for a spherical wave. One would expect that for our range of 9.66 km, while using a source with a collimated beam, the plane wave prediction would be better, also because the phase of a wavefront is only varying about 1/50 of the wavelength (0.9 μm) over the MSRT pupil (with a diameter of 38 mm). If we would chose as C_n^2 fit line: $\log(C_n^2)=-0.347*ASTD-16.13$, and for SI: $SI=25.4*10^{14}*C_n^2$, the correspondence between the measured data with the plane wave prediction would be much better.

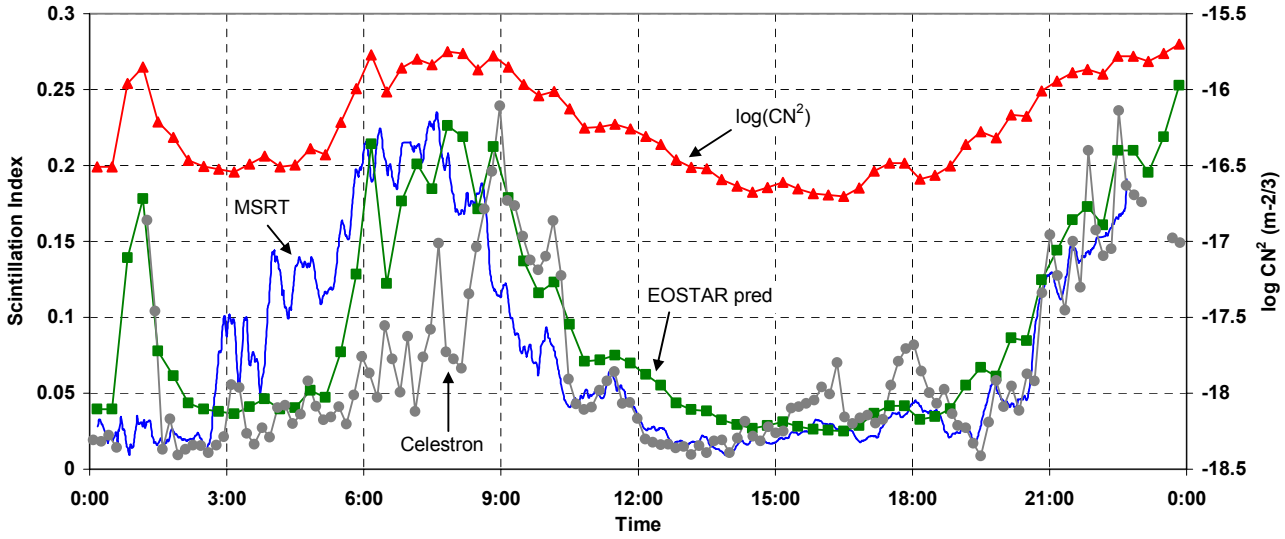

Figure 11. Comparison of measured and predicted SI data for 5 June; also shown is $\log(C_n^2)$ obtained via the ASTD

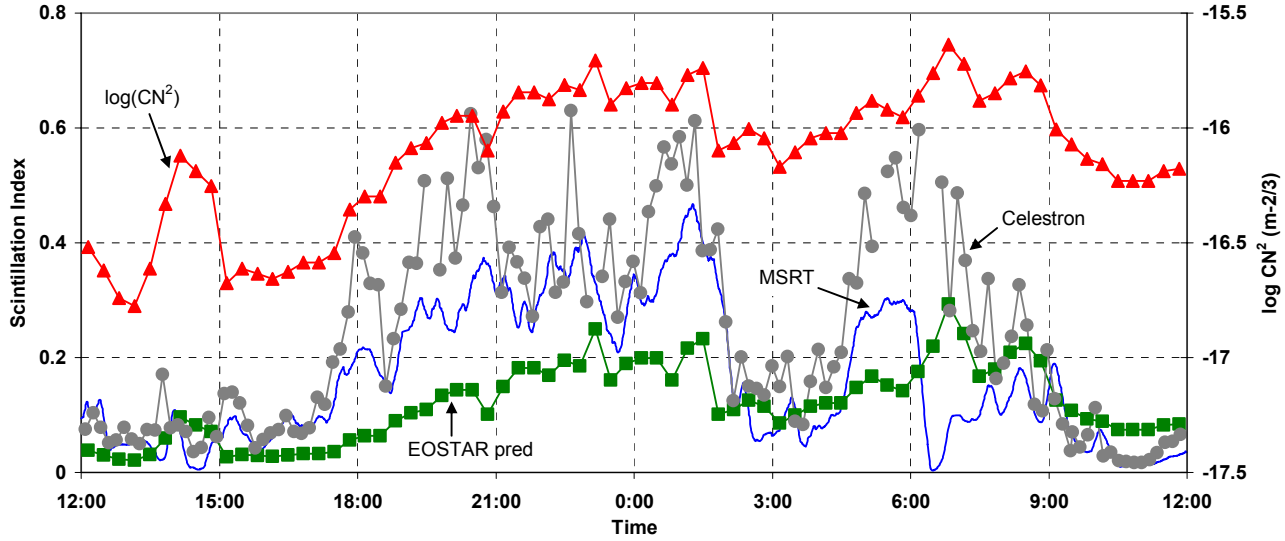

Figure 12. Comparison of measured and predicted SI data for 11/12 June; also shown is $\log(C_n^2)$ obtained via the ASTD

A comparison of SI data, measured with the MSRT transmissometer and the Celestron camera and data, predicted with the modified EOSTAR model and our "fit" relation, while using the measured ASTD data at Roman Rock, is shown for two periods in Figures 11 and 12. The figures also show the behaviour of $\log(C_n^2)$, directly obtained from the ASTD; the value of C_n^2 is apparently fluctuating around 10^{-16} ($m^{-2/3}$). We find that the SI values, measured with the Celestron and the MSRT system, are rather similar, although both systems are measuring in opposite directions, have a different pupil size (125 resp. 38 mm) and a different integration time (0.1 resp. 10 ms). The SI of the Celestron was obtained by taking the integrated intensity for all pixels in the blur spot for each of a series of 50 frames. The (subtracted) background intensity level was low due to the short exposure time. The average and standard deviation of the series of 50 consecutive frames delivered every 10 minutes an SI data point. The correspondence between both measured data sets is less for the 5th of June before 08.00, because of some saturation problems. The EOSTAR prediction fails somewhat (factor 2 lower than measured) on the 11th of June after 17.00, when the windspeed is decreasing to values below 2 m/s. A similar behavior happens on the 12th from 04.30 to 06.00. It is recommended to include in future predictions the effect of windspeed.

The effect of showers on transmission (Tau) and SI is illustrated in Figure 13 with examples on 4, 7 and 9 June. The data are sampled here with a sampling rate of 0.25 Hz. The plots show, that Tau and the SI are simultaneously decreasing rapidly when it starts to rain. When the rain stops, Tau increases and SI sometimes increases and sometimes stays at low values. One of the reasons for this behavior may be that the atmospheric turbulence in the path is strongly reduced by the rain, as if the energy of the eddies is absorbed by the shower. We have to realise however, that most of the showers were falling locally, not occupying the whole path. Therefore it cannot be excluded, that forward (incoherent) scattering by the raindrops in the measurement volume, contributes to the strong reduction of SI.

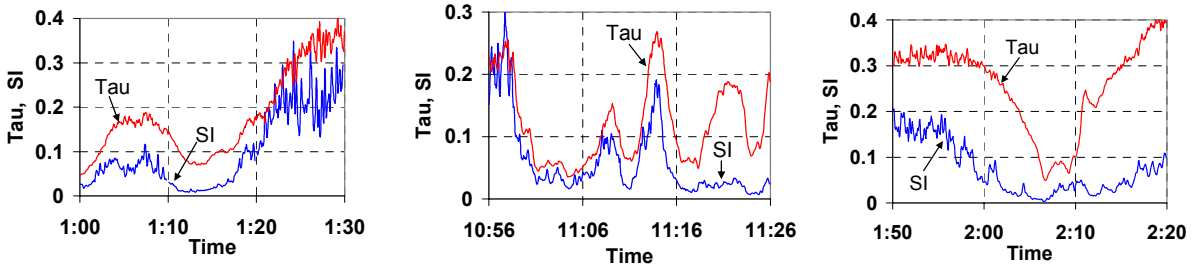

Figure 13. Examples of the effect of showers on the transmission (Tau) and scintillation index (SI) for showers on 4 June (left), 7 June (centre) and 9 June (right), measured with the MSRT for the 0.9 μm channel; averaging time: 10 s

Examples of blur measurements, carried out with the Celestron camera, are shown in Figure 14. The measured data were obtained by calculating the centre of "gravity" (x and y) of the blur spots for each frame of the series of 50 full frames (actually 100 half-frames), taken every 10 minutes. The mean values of x and y were taken (x_c and y_c), while the mean beam wander BW was calculated from the relation: mean-BW=$<\{(x-x_c)^2+(y-y_c)^2\}^{0.5}>$. As stated before, we assume the beam wander to be representative for the total blur in this case. It is noted, that BW is the radius of the blur spot; the real blur diameter, responsible for the resolution is more related to twice the standard deviation of BW for each series of 100 half-frames. It appears however that 2*std-BW≈mean-BW, which we will call here the measured blur. We performed bulk model predictions (Smith/Paulson) via the fit line in Figure 9 (centre): blur=-16*ASTD+55 (μrad). In Figure 14 we have included these predictions by taking the ASTD data at Roman Rock. The predicted blur corresponds well with the measured data. Typical deviations are found on the 5th of June around 15.00 and on the 13th of June around 13.00; in these periods the air temperature increases, while the relative humidity decreases, apparently giving rise to the measured blur, exceeding the predicted blur with about 50%.

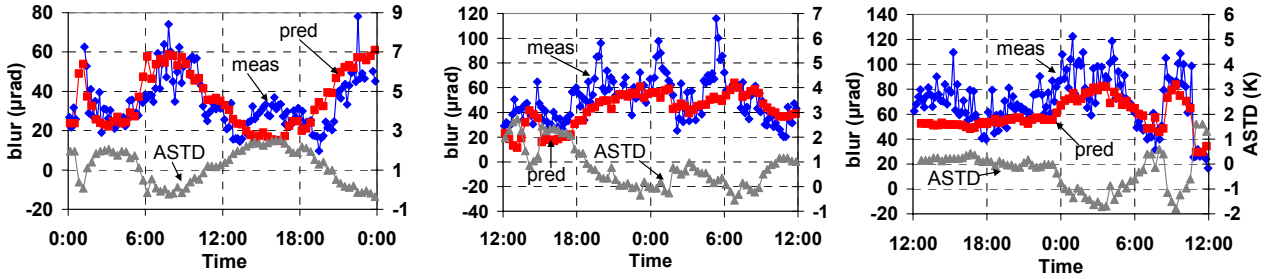

Figure 14. Results of measured blur data for 24 hour periods on 5 June (left), 11/12 June (centre) and 13/14 June (right); also shown are blur data predicted from ASTD data by via the fit line in Figure 9 (centre)

6. DISCUSSION, SUMMARY

In this paper we have presented results from optical propagation measurements in the False Bay. The data were used for validation of models concerning the vertical temperature profile, aerosol extinction and turbulence effects. The primary model, as used in EOSTAR, was a derivative of the bulk model, using simple environmental input data. The refraction measurements delivered Angles of Arrival for a range of 15.7 km, that were well simulated by an empirical temperature profile: $T=a*h^n$ with n=1.5 and T'/T=0.15 at 10 m height. The Smith variant of the bulk model, with Paulson's stability functions, performed reasonably well, except for conditions with positive Air to Sea Temperature Difference (ASTD). From the multiband transmission measurements we retrieved particle size distributions (Junge type), with preference to the data from the 0.9 and 1.5 μm bands. From these size distributions, transmissions in other spectral bands (including IR) can be obtained, when proper humidity data are taken into account. The high sampling rate of the transmission data allowed detailed analysis of the temporal effects, such as showers and gravity waves. The Fourier spectrum showed a moderate to low drop-off of the amplitude with frequency, compared to the theoretical Kolmogoroff temporal spectrum. Correlation coefficients of the signals of neighboring entrance pupils were determined and found to increase linearly with the log of integration time. It was shown, that the data samples followed a typical log amplitude behavior. The ratio of the maximum signal level and the average signal level (max/avg) was compared to the ratio of the standard deviation and the average signal level (std/avg): max/avg=6.89*std/avg+0.38, which relation holds for all data during the trial.

Special attention was spent on the effect of turbulence by the collection of data on scintillation and beam wander. In the bulk model a dip is predicted in plots of scintillation and blur versus ASTD for an ASTD of 0.75 K. This dip is not found in the measured data, probably because of variations of ASTD along the measurement path. If we take for the prediction of the Scintillation Index (SI) $SI=12.7*10^{14}*C_n^2$, where C_n^2 is related to ASTD by: $\log(C_n^2)=-0.347*ASTD-15.83$, the measured and predicted SI data match quite good. The latter approximation represents a kind of smoothing effort in the bulk prediction, where it is noted that for the stability functions the Kondo version has to be taken. It was found, that in contrary to the bulk prediction, SI is increasing when the wind speed decreases to levels below 3 m/s. It was also shown, that during showers, the SI and the transmission level decrease simultaneously in a similar manner. SI values measured with the Celestron camera and the MSRT were matching quite good, although for both systems the integration times and the pupil averaging were different. The blur, measured with the Celestron, was compared to predictions from the bulk

model by the linear relation: blur=-16*ASTD+55 (μrad), which is also smoothing the dip in the bulk model, where the Paulson stability functions did perform better in this case. Measured and predicted blur matched surprisingly good for three days without showers. We finally want to thank Willem Gunter and George Vrahimis from IMT (Simonstown) for their support and for providing data from their weather station. From TNO-DSS we thank Herman Bekman and Koen Benoist for providing software for data analysis and processing and Leo Cohen for preparing and testing the MSRT.

REFERENCES

[1] Piet B. W. Schwering et al, *Optical characterisation of small surface targets*, SPIE Vol. 6739, Electro-Optical Remote Sensing, Photonic Technologies and their Applications, Florence, September 2007

[2] Arie N. de Jong et al, *Refraction measurements and modeling over the Chesapeake Bay during the NATO (TG51) SAPPHIRE trials, June 2006*, SPIE Vol. 6747, Optics in Atmospheric Propagation and Adaptive Systems, Florence, September 2007

[3] Arie N. de Jong et al, *The use of multi-band transmission data, collected at Scripps pier in November 2006, for the investigation of aerosol characteristics*, SPIE Vol. 6708, Atmospheric Optics: Models, Measurements and Target-in-the-Loop Propagation, San Diego, August 2007

[4] Arie N. de Jong et al, *Aerosol size distributions, retrieved from multi-band transmissometer data in the Southern Baltic Sea during the VAMPIRA trials*, SPIE Volume 6364, Optics in Atmospheric Propagation and Adaptive Systems
IX, Stockholm, September 2006

[5] Arie N. de Jong et al, *TG16 point target detection experiment POLLEX, Livorno 2001,* SPIE Volume 4820, Infrared Technology and Applications XXVIII, Seattle, July 2002

[6] Arie N. de Jong et al, *Investigation of aerosol particle size distribution in the San Diego Bay by means of multi-band transmissometry,* SPIE Volume 6303, Atmospheric Optical Modeling, Measurement and Simulation II, San Diego, August 2006

[7] Arie N. de Jong et al, *Two-way multi-band optical/IR transmission measurements in the Persian Gulf-Coastal region*, SPIE Volume 5981, Optics in Atmospheric Propagation and Adaptive Systems VIII, Bruges, September 2005

[8] Kenneth Anderson et al, *The RED Experiment: An Assessment of Boundary Layer Effects in a Trade Winds Regime on Microwave and Infrared Propagation over the Sea*, Proc. American Meteorological Society, September 2004

[9] Gerard J. Kunz et al, *EOSTAR: an electro-optical sensor performance model for predicting atmospheric refraction, turbulence and transmission in the marine surface layer*, SPIE Volume 5237, Optics in Atmospheric Propagation and Adaptive Systems VI, Barcelona, September 2003

[10] Arie N. de Jong et al, *Atmospheric refraction effects on optical/IR sensor performance in a littoral-maritime environment*, Applied Optics, Vol. 43, No. 34, 1 December 2004

[11] Arie N. de Jong, *Refraction effects of atmospheric inhomogeneities along the path*, SPIE Vol. 5237, Optics in Atmospheric Propagation and Adaptive Systems VI,Barcelona, September 2003

[12] Arie N. de Jong, *Enhanced IR point target detection by atmospheric effects,* SPIE Vol. 4820, Infrared Technology and Applications XXVIII, Seattle, July 2002

[13] Arie N. de Jong et al, *Multi-band optical/IR transmissometry during the VAMPIRA trials, spring 2004*, SPIE Volume 5572, Optics in Atmospheric Propagation and Adaptive Systems VII, Gran Canaria, September 2004

[14] Arie N. de Jong, *Intensity variations of small airborne incoming targets, popping-up above the horizon*, SPIE Vol. 5237, Optics in Atmospheric Propagation and Adaptive Systems VI, Barcelona, September 2003

[15] Arie N. de Jong et al, *Point target extinction and scintillation as function of range at LAPTEX, Crete*, SPIE Volume 3125, Propagation and Imaging through the atmosphere, San Diego, July 1997

[16] Arie N. de Jong et al, *Low elevation transmission measurements at EOACE, Part III: Scintillation Effects*, SPIE Volume 3125, Propagation and Imaging through the atmosphere, San Diego, July 1997

[17] Arie de Jong et al, *Scintillation measurements during the EOPACE November '96 and August '97 campaigns*, SPIE Volume 3433, Propagation and Imaging through the atmosphere, San Diego, July 1998

[18] Jacques Claverie et al, *Refraction effects under stable conditions in coastal environments,* SPIE Volume 6747, Optics in Atmospheric Propagation and Adaptive Systems X, Florence, September 2007

[19] Robert R. Beland, *Propagation through Atmospheric Optical Turbulence*, The Infrared & Electro-Optical Systems Handbook, Volume 2, SPIE Optical Engineering Press, 1993